National Conference with International Participation
ENGINEERING MECHANICS 2007
Svratka, Czech Republic, May 14 – 17, 2007

UNSTEADY CHARACTERISTICS OF A PLANE JET IMPINGING INTO A BLIND TROUGH CAVITY

M. Knob[*], P.Antoš[*], L. Popelka[*], P. Šafařík[**], J. Adamec[**]

Summary: *In this contribution, the unsteady character of a jet blown into a blind trough cavity is presented; the investigation is performed both experimentally and numerically. The numerical investigation is performed using a commercial package Fluent 6.2, while the experimental investigation is performed by means of both the hot wire anemometry and the TR PIV. The phenomenon was investigated in the range of the jet- hydraulic- diameter- based Reynolds numbers between 30000 and 20000, the cavity aspect ratios 2:3 and 3:4 and, finally, for impingement angles between 0 and 15°. It is explained in detail, that the jet swinging phenomenon is caused by the double Coanda effect.*

1. Introduction

In a blind cavity, subjected to a jet impingement (see. Fig. *1*) the jet swinging effect has been known for decades (see. e.g. [*1*] or [*5*]), however, the correct physical explanation has remained questionable. Although each author of the limited number of reports on this topic gave some basic idea of the jet swinging mechanism, none of the are fully acceptable- they are either half- baked, or physically incorrect ([*5*]).
Molloy and Taylor ([*1*]) have only reported the fact of the oscillations, but they did not even try to give any explanation of the switching mechanism. The fact of the flow- field oscillations was demonstrated by results of extensive flow- visualisation work.
After a long time, Shakouchi et. al. ([*2*]) returned to their work, performing both the experimental and the numerical research. Their experiments were performed on a plexi-glass model, so that no new experimental facility would be made for flow visualisation experiments. In the somewhat void paper they conclude, that the main mechanism is in the interaction of a pair of vortices, which are formed in the cavity. As explained below, this conclusion is irrelevant.
After another twenty years, Mataoui et. al. ([*3-5*]) published several papers on this problem. The excessive work, both the experimental and numerical, is coronated by a development of a semi- analytical relation for the jet- switching frequency. This model is based on the pressure conditions in the vicinity of the impingement point, which is indeed a good idea, but since the mechanism lays somewhere else, the results can not be relevant. Describing all the unconsidered circumstances lays outside the scope of this paper, lets therefore only mention

[*] Ing. Martin Knob, Ing. Pavel Antoš, Ing. Lukáš Popelka: Institute of Thermomechanics ASCR, v.v.i., Dolejškova 1402/5, 182 00, Praha 8; tel. +420 266 053 313, knob@it.cas.cz
[**] Prof. Ing. Pavel Šafařík, CSc., Doc. Ing. Josef Adamec, CSc.: CTU in Prague, Faculty of Mechanical Engineering, Technická 4, 166 07 Praha 6

the fact, that the switching frequency, predicted by his model, does not depend on the aspect ratio of the cavity, which is an obvious nonsense.
Gillard and Brizzi ([*6*]) investigated a similar problem, their cavity was, however, not rectangular.

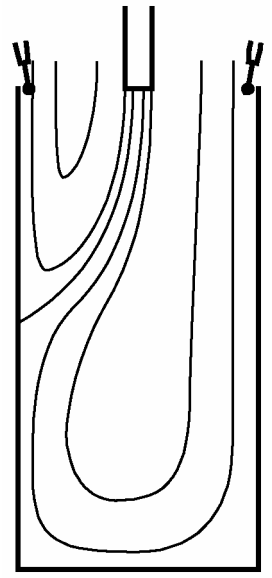

Fig. 1: The blind cavity subjected to a jet impingement; with the position of the two hot wire probes

Another investigation was performed by Dyban et. al. This included the flow visualisations of the impingement into both the parabolic and the rectangular cavity. In their work, the cavity outlets have not been opened to the atmosphere, but they lead the fluid into two outlet channels, on which the control valves were installed- this is a crucial point of their work, since they concluded, that the oscillatory behaviour of the flow- field is caused by the influence of the control valves, namely by the increase of the static pressure in the outlet channel, corresponding to the impingement side of the jet. However, as proved by recent research, the oscillatory phenomenon occurs even in a cavity, the outlet of which is opened to the atmosphere and therefore, Dyban's conclusion is not correct.
Some more reports can be found, see e.g. Sobeiski and Badur ([*8*]) or Dvořák et. al. ([*9*]), however the reports either do not give any results (*8*), or model only a steady flow field (*9*).
Last but not least, the physically correct explanation of the above mentioned phenomenon is presented e.g. in [*10*]. It is caused by the interaction between the injected fluid and the quasi wall jets, created after the impingement of the fluid onto either the cavity bottom or one of the side walls.

2. The Investigation Procedure

The investigation was performed both numerically and experimentally.

2.1 Numerical Investigation

The numerical investigation is being performed using a commercial package Fluent *6.2*. For the various jet- hydraulic- diameter- based Reynolds numbers, impingement angles and cavity aspect ratios, suitable grids were created, however, the number of *40000* cells was kept.
As mentioned above, the computational grid consisted of *40000* cells. Furthermore, the standard k-ε model of turbulence, the second order time- marching scheme and the second order upwind scheme were applied. The PISO algorithm was used.

2.2 Experimental Investigation

The experimental investigation was performed by means of both the hot wire anemometry and TR PIV.

2.2.1 The Hot Wire Anemometry

For the purpose of experimental investigation by means of the hot wire anemometry, two hot wire probes for simultaneous velocity measurement were used- each of them was placed on one side of the cavity opening, see Fig. *1*; this enables the quantification of the phenomena occurring in the region of interaction of the jet and a wall jet as described below. The reduced number of measurements together with sufficient amount of information are the main advantages of such a measurement.

2.2.2 The TR PIV

For the investigation of the whole flow field, the standard Dantec TR PIV system, available at the Institute of Thermomechanics ASCR, v.v.i., was used. As the seeding particles, droplets of glycerol solution in water of the average diameter of about *2 μm* were used.

For all the investigated regimes, the interrogation areas were set to the size of *64x64* pixels due to large areas with lack of particles, created by intensive fluid entrainment effect in the vicinity of the jet exit, see. Fig. *2*. Since the correlation between the two signals at each side of the cavity opening was one of the points of interest, the interrogation areas needed to be enlarged as much as possible in order to find sufficient number of particles inside.

For each Reynolds number, different time delay between pulses of *25 μs* for *Re= 3000*, *12 μs* for *Re=11200* and *6 μs* for *Re= 19600* were set; these values ensure the best results for given size of the interrogation areas.

The results, obtained by the PIV have been subject to several investigation procedures. First, the sequences of successive images have been observed in order to examine the unsteady behaviour of the flow field. Second, similarly to the hot wire measurements, the time record in two points at each side of the cavity opening were evaluated. Last but not least, in order to study the dynamic behaviour of the system, the biorthogonal decomposition was applied.

The biorthogonal decomposition was first defined by Aubry et. al. ([*11*]). This method is based on the properties of both the spatial and the temporal correlation operator. It can be shown, that these two correlation operators have the same eigenvalues. Then the spatiotemporal signal $\vec{U}(\vec{x},t)$ can be decomposed into the following sum:

$$\vec{U}(\vec{x},t) = \sum_i \lambda_i \mu_i(t) \vec{\Psi}_i(\vec{x}) \qquad (1)$$

where λ_i are the eigenvalues of (both) the correlation operators, the μ_i are the eigenfunctions of the temporal correlation oparator and $\vec{\Psi}_i$ are the corresponding eigenmodes of the spatial correlation operator. In the decomposition, the μ_i play a role of a time sequence (and are therefore called *chronos*), while the $\vec{\Psi}_i$ play a role of (time constant) vector fields (and are called *topos*). Clearly, using this decomposition, the vector spatiotemporal signal is decomposed into a sum of some "typical" vector fields (*topos*), having some time history (*chronos*), weighted by a coefficient λ, which, with respect to the definition of the correlation operators, has the physical meaning of energy, contained in each of the *topos*. Once sorted in descending order according to the eigenvalues (i.e. the energy in each eigenmode), the sum of first *5* terms contains more than *85%* of total energy in the studied case, while the sum of first *10* terms contains more than *90%* of energy, see Fig. *3*.

Some additive information on the set of *chronos* and *topos*, like the (statistical) entropy is not considered in this case.

3. Results and discussion

On the Figs. *4-9*, the time record of the flow field for the regime α*= 0°*, aspect ratio *3:4*, *Re= 11200*, is shown. It is obvious, that the jet swings between the side walls in a periodic manner. In order to demonstrate the properties of the biorthogonal decomposition, the Figs. *10-15* show the set of the first five *chronos*, plus the tenth one. Obviously, the most energetic modes exhibit a nearly periodic behaviour and, as the energy contained in each mode decreases, the

periodicity is less and less evident, until it vanishes completely, as could be by the way expected.
The set of *topos* exhibits a similar behaviour. The most energetic structures contain larger structures, which can not surprise. For the readers view, the set of the first five plus the tenth *topos* is shown on the Figs. *16-21* together with their curl, see Figs. *22-27*.

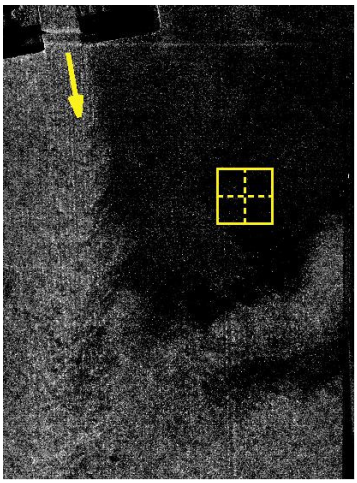

Fig. 2: The area with lack of particles; the size of interrogation area 32x32 px marked by dashed line; 64x64 marked by solid line

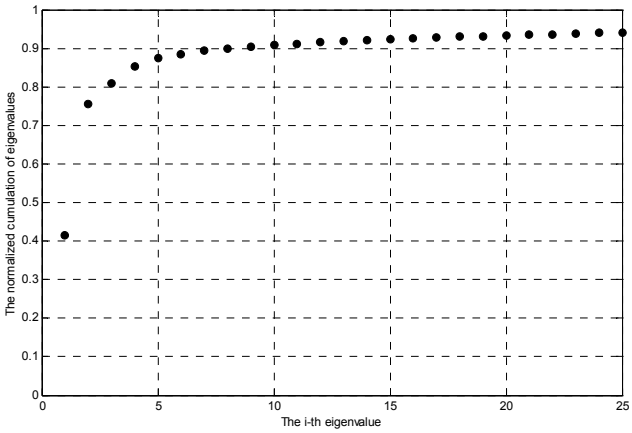

Fig. 3: Normalized cumulative sum of the first 25 (common) eigenvalues of both the spatial and temporal correlation oparator; the first 5 eigenvalues contain more than 85% of energy

4. Conclusions

The phenomenon of jet swinging is caused by the double Coanda effect; the fluid enters the cavity through a jet, placed at the cavity opening. Then it impinges one of the walls and spreads along the side walls upwards, i.e. back to the cavity opening. At that moment, it starts to interact with the fluid, being ejected from the nozzle. In the area of interaction, an under pressure zone is created and, consequently, the jet is bent towards to opposite side wall. The interaction of these can be called the double Coanda effect.
As the result of the above described process, certain structure in the flow field is created. This structure can be studied in detail using the biorthogonal decomposition. As demonstrated by the results on the Fig. *16*, a large vortex is created inside the cavity, the rotational direction of which alternates, following the course shown on the Fig. *10*. This vortex is connected with the jet swinging. In addition to this vortex, some additional structures, shown on the other pictures are found in the flow field, so that the signal with all its details is reconstructed.

5. Acknowledgement

This work was supported by the grant GA AVČR IAA2076403.

6. References

[1] Molloy, N.A., Taylor, P.L. *Oscillatory Flow of a Jet into a Blind Cavity*, Nature, 1969
[2] Shakouchi, T., Suematsu, Y., and Ito, T. *A Study on Oscillatory Jet in a Cavity*, Bulletin of the JSME, 1982

[3] Mataoui, A., Schiestel, R. and Salem, A. *Flow Regimes of a Turbulent Plane Jet into a Rectangular Cavity: Experimental Approach and Nuemrical Modelling,* Flow, Turbulence and Combustion, 2001
[4] Mataoui, A., Schiestel, R. and Salem, A. Oscillatory Phenomena of a Turbulent Plane Jet Flowing Inside a Rectangular Cavity, *Proceedings of Advances in Fluid Mechanics*, 2002
[5] Mataoui, A., Schiestel, R. and Salem, A. *Study of the Oscillatory Regime of a Turbulent Plane Jet Impinging in a Rectangular Cavity*, Applied Mathematical Modelling, 2003
[6] Gilard, V. and Brizzi, L.-E. Velocity Field in the Vicinity of a Slot Jet Impinging a Curved Wall, *Online Proceedings of the International Symposium of Laser Measurement Techniques*, 2002.
[7] Dyban, E.P., Mazur, A.I., Epik, E.Ya: *Discharge of a Plane Air Jet Into a Blind Pass*, Journal of Engineering Physics and Thermophysics, 1971
[8] Sobieski, W. and Badur, J.: *Forms of Unsteady Flow in a 2-D Channel*, PAMM 2005
[9] Dvořák, R., Trávníček, P., Vogel, J.: Impaktní proud v polouzavřeném prostoru, Proceedings of the Seminar Topical Problems of Fluid Mechanics, 2000
[10] Knob, M., Antoš, P., Adamec, J.: *The Unsteady Behaviour of a Jet Impinging into a Trough Cavity*, Proceedings of the Colloquium Fluid Dynamics, 2006
[11] Aubry, N., Guyonnet, R. and Lima, R.: *Spatiotemporal Signal Analysis of Complex Signals: Theory and Applications*, Journal of Statistical Physics, 1991

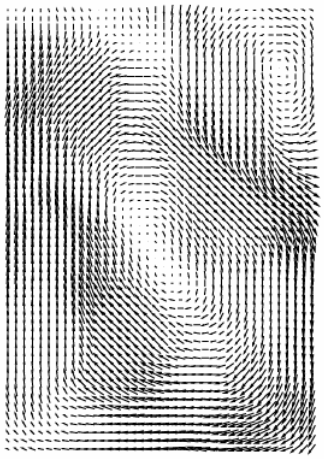

Fig. 4: The instantaneous flow field, α= 0°, 3:4, Re=11200, t=0,224 s

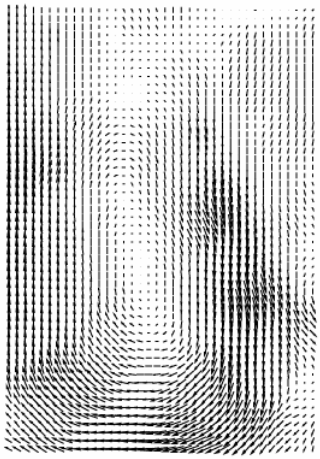

Fig. 5: The instantaneous flow field, α= 0°, 3:4, Re=11200, t=0,232 s

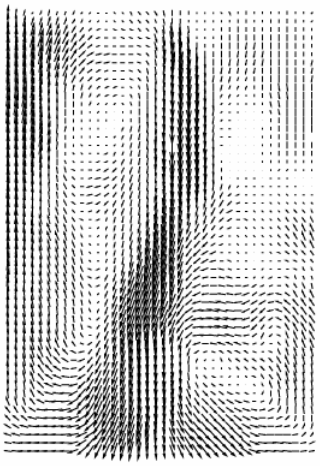

Fig. 6: The instantaneous flow field, α= 0°, 3:4, Re=11200, t=0,240 s

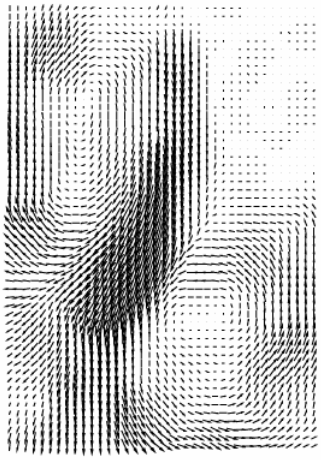

Fig. 7: The instantaneous flow field, α= 0°, 3:4, Re=11200, t=0,248 s

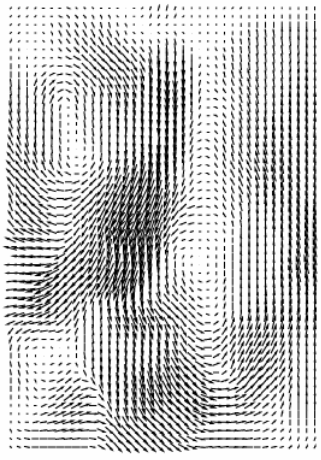

Fig. 8: The instantaneous flow field, α= 0°, 3:4, Re=11200, t=0,256 s

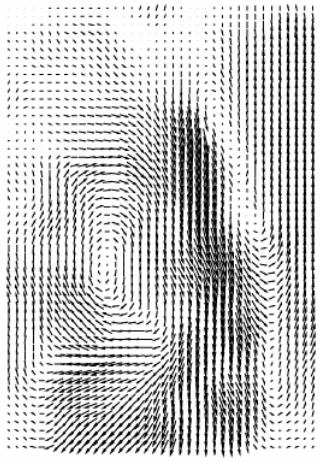

Fig. 9: The instantaneous flow field, α= 0°, 3:4, Re=11200, t=0,264 s

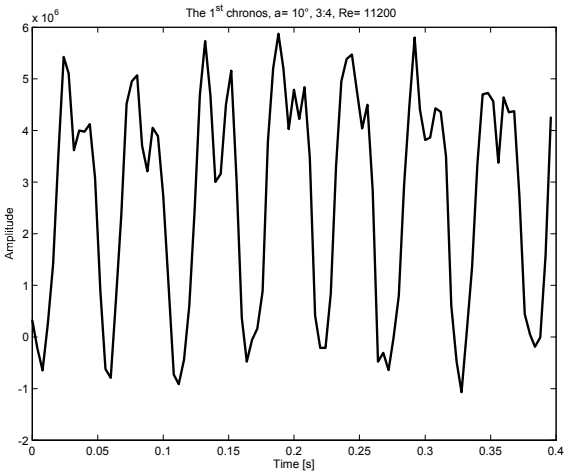

Fig. 10: The first 100 samples of the first CHRONOS multiplied by its eigenvalue; α= 10°, 3:4, Re= 11200

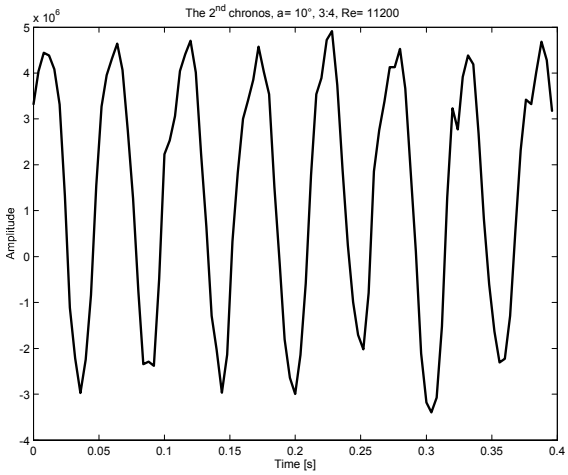

Fig. 11: The first 100 samples of the second CHRONOS multiplied by its eigenvalue; α= 10°, 3:4, Re= 11200

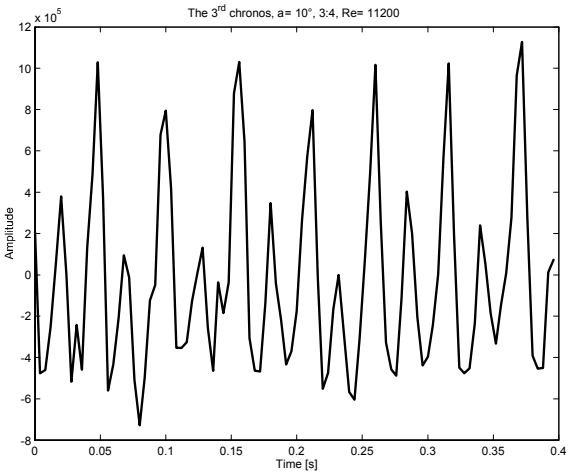

Fig. 12: The first 100 samples of the third CHRONOS multiplied by its eigenvalue; α= 10°, 3:4, Re= 11200

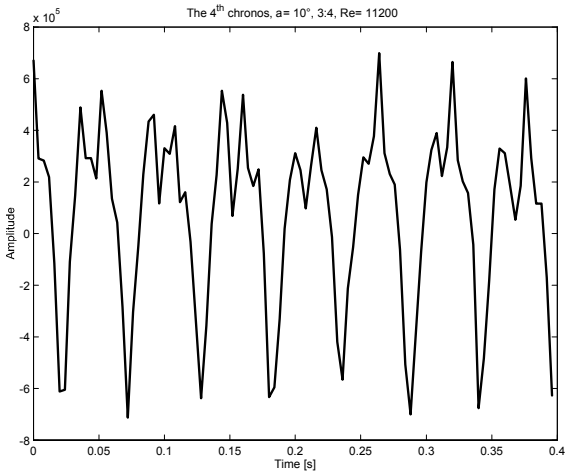

Fig. 13: The first 100 samples of the fourth CHRONOS multiplied by its eigenvalue; α= 10°, 3:4, Re= 11200

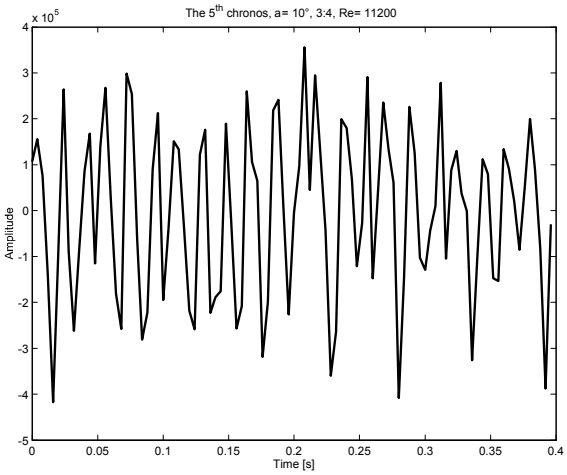

Fig. 14: The first 100 samples of the fifth CHRONOS multiplied by its eigenvalue; α= 10°, 3:4, Re= 11200

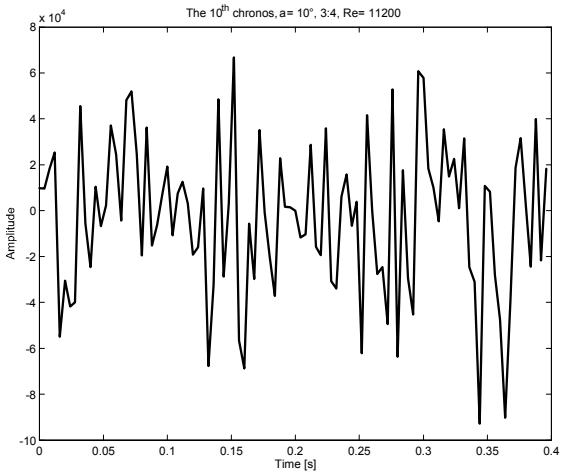

Fig. 15: The first 100 samples of the tenth CHRONOS multiplied by its eigenvalue; α= 10°, 3:4, Re= 11200

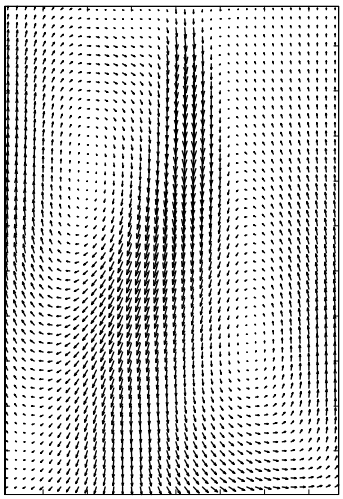

Fig. 16: The first TOPOS; α= 10°, 3:4, Re= 11200

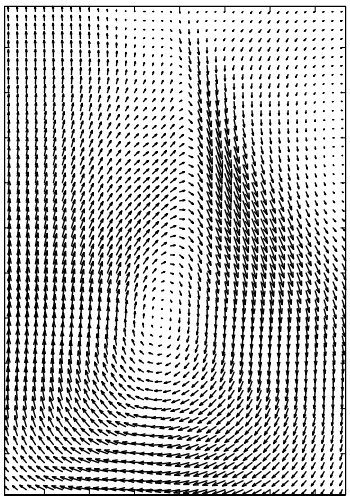

Fig. 17: The second TOPOS; α= 10°, 3:4, Re= 11200

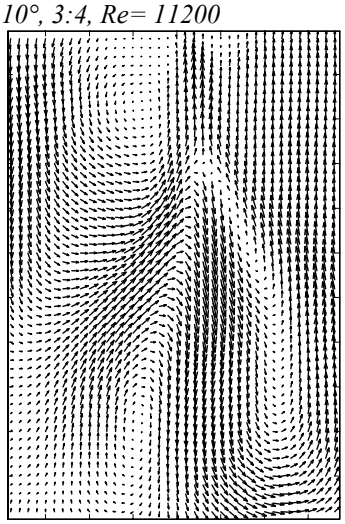

Fig. 18: Thethird TOPOS; α= 10°, 3:4, Re= 11200

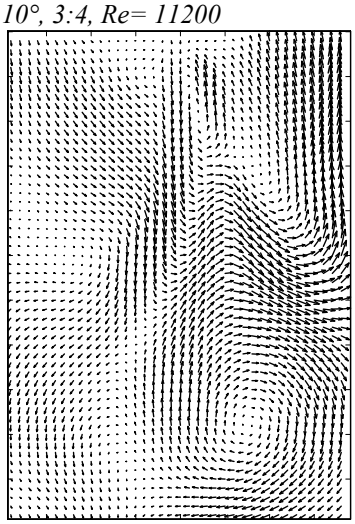

Fig. 19: The fourth TOPOS; α= 10°, 3:4, Re= 11200

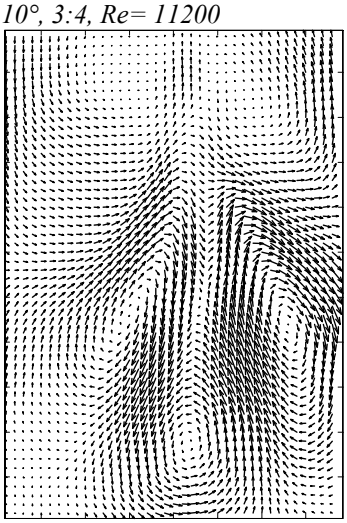

Fig. 20: The fifth TOPOS; α= 10°, 3:4, Re= 11200

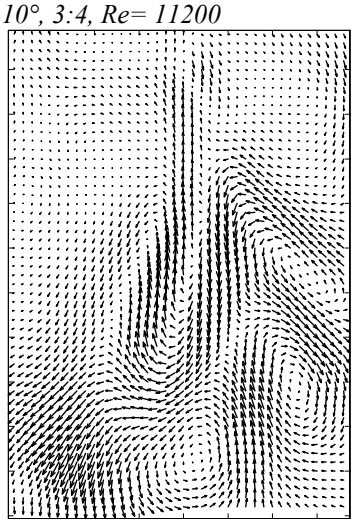

Fig. 21: The tenth TOPOS; α= 10°, 3:4, Re= 11200

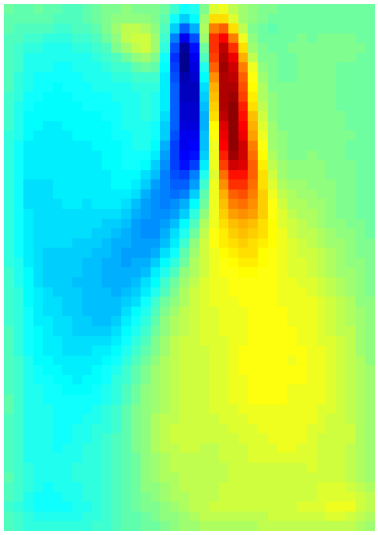

Fig. 22: The curl of the first TOPOS; α= 10°, 3:4, Re= 11200

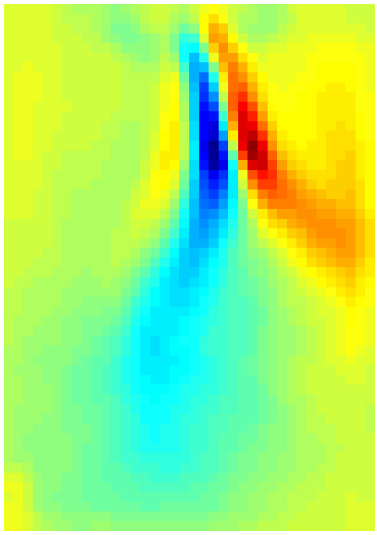

Fig. 23: The curl of the second TOPOS; α= 10°, 3:4, Re= 11200

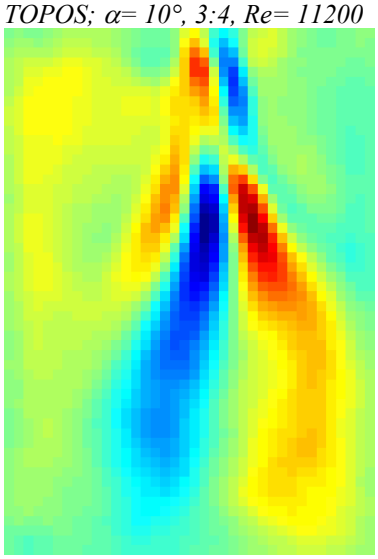

Fig. 24: The curl of the third TOPOS; α= 10°, 3:4, Re= 11200

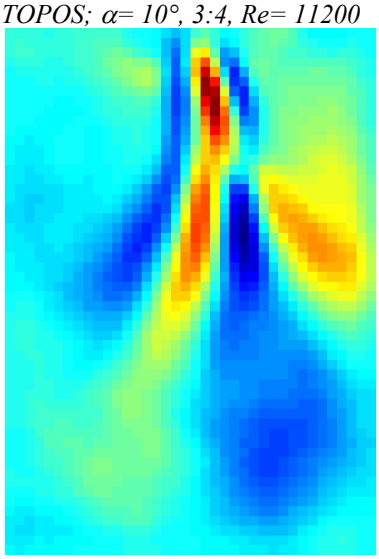

Fig. 25: The curl of the fourth TOPOS; α= 10°, 3:4, Re= 11200

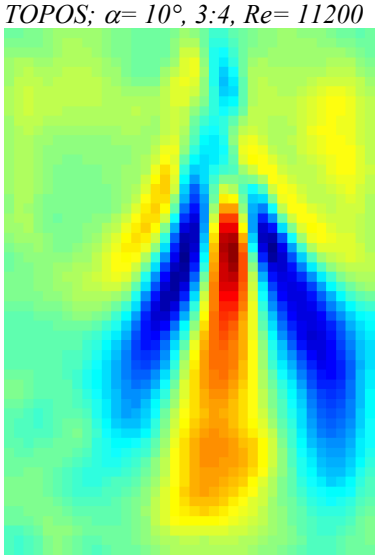

Fig. 26: The curl of the fifth TOPOS; α= 10°, 3:4, Re= 11200

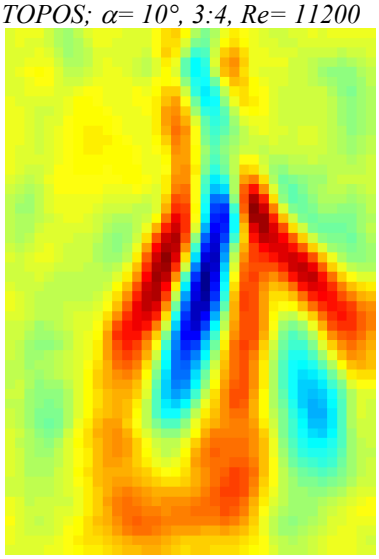

Fig. 27: The curl of the tenth TOPOS; α= 10°, 3:4, Re= 11200